Bachelor's Thesis

Kinematische Rekonstruktion von t$\bar{\text{t}}$ Ereignissen im dileptonischen Endzustand

Kinematic Reconstruction of t$\bar{\text{t}}$ Events in the Dileptonic Final State

prepared by

Maximilian Stephan Kurjahn

from Parchim

at the II. Physikalisches Institut

Zusammenfassung

Das Top-Quark ist das schwerste Teilchen im Standardmodell. Es kann über ein W-Boson in ein geladenes Lepton, ein Neutrino und ein b-Quark zerfallen. Im dileptonischen $t\bar{t}$-Event ist die kinematische Rekonstruktion aufgrund der zwei nicht detektierbaren Neutrinos herausfordernd. Um die verbleibende Ambiguität in der Berechnung des Neutrinoimpulses zu lösen, wird der Neutrino-Gewichtungsalgorithmus verwendet.

In dieser Bachelorarbeit ist für eine höhere Schwerpunktsenergie von $\sqrt{s} = 13\,\text{TeV}$ des Large Hadron Colliders (LHC) die Neutrino-Pseudorapiditätsverteilung aktualisiert worden. Des Weiteren wird eine neue Methode zum Lösen der Ambiguität in dem Neutrinoimpuls vorgestellt. Diese neue Methode zeigt eine bessere Performanz und Rekonstruktionseffizienz. Die volle kinematische Rekonstruktion des dileptonischen $t\bar{t}$-Systems kann somit erreicht werden und präzisere Top-Quark-Messungen sind möglich.

Stichwörter: Kinematische Rekonstruktion, Top-Quark, Neutrino-Gewichtung

Abstract

The top quark is the heaviest particle in the Standard Model. It can decay via a W-boson into a charged lepton, a neutrino, and a b-quark. In the $t\bar{t}$ dilepton event, the kinematic reconstruction is challenging due to the undetectable neutrinos. For that, the Neutrino Weighting Algorithm is applied to solve the remaining ambiguity in the calculation of the neutrino momentum.

In this bachelor thesis, the neutrino pseudorapidity distribution is updated for a higher centre-of-mass energy of $\sqrt{s} = 13\,\text{TeV}$ at the Large Hadron Collider (LHC). Furthermore, a new method for solving the ambiguity in the neutrino momentum is presented. This new method shows a better performance and reconstruction matching efficiency. The full kinematic reconstruction of the $t\bar{t}$ dilepton system can thus be reached, and more precise top quark measurements are possible.

Keywords: Kinematic reconstruction, top quark, neutrino weighting

Contents

1 Introduction

To understand the fundamental principles and physics of the Universe, one needs to research the constituent particles our world is made of. Elementary particle physics describes these constituents and how they interact with each other. The Standard Model (SM) of particle physics is the theory that predicts the behaviour of these fundamental particles very well.

Therefore, large experimental setups are required in order to allow measurements at high energies. The largest one ever built by human kind is the Large Hadron Collider (LHC), which is located at Cern (Conseil européen pour la recherche nucléaire), Geneva. At this particle accelerator, protons or heavier ions are collided to produce such fundamental particles, e.g. a quark-antiquark pair. Scientists from all around the world have access to these events and analyse them to test existing theories and also to look for new physics beyond the Standard Model.

The top quark is the heaviest particle in the SM. Due to its large mass, it has an extremely short lifetime and therefore it decays before hadronisation. Thus, it transfers its properties to the daughter particles and provides us with the opportunity to study the properties of a "bare" quark. The top quark decays almost exclusively into a bottom quark and a W-boson, the latter of which decays further into a light quark-antiquark pair or into a charged lepton and its corresponding neutrino.

The reconstruction of the $t\bar{t}$ system, where both W-bosons decay leptonically, is the focus of this thesis. For that, a kinematic reconstruction algorithm is used, since a precise reconstruction of the top quark is crucial for many precision measurements in top quark physics. Furthermore, the neutrinos that are produced in the collision cannot be detected directly and appear as missing energy in the transverse plane.

In cases where there is just one neutrino in the final state, the missing transverse energy can be assigned to the undetected neutrino. However, a reconstruction method for the momentum along the beam axis is still required. In the case of two neutrinos, the dilepton channel, even the ambiguity of the momentum of the neutrinos in the transverse plane

remains. Therefore, kinematic assumptions are necessary. One uses the distribution of the angle between the neutrino and the beam axis in order to solve for this ambiguity of the neutrino momentum.

Chapter 2 introduces the SM of elementary particle physics, with particular emphasis on the top quark. Chapter 3 describes the experimental setup – the LHC and the ATLAS detector. The approach on how to reconstruct the $t\bar{t}$ event and especially the two neutrinos is discussed in Chapter 4. The results can be found in Chapter 5. Finally, Chapter 6 concludes the thesis and presents an outlook for future analysis.

Natural units $\hbar = c = 1$ are used throughout this thesis.

2 The Standard Model

The Standard Model (SM) unifies three of the four known fundamental forces and describes very well the behaviour of all the fundamental particles. It was developed in the second half of the twentieth century [1–7] and predicted successfully some new particles, which were not discovered at that time. For example, the tau neutrino, the Z- and W-bosons, and the Higgs boson, which was just discovered a few years ago (July 2012) [8, 9]. This chapter is based on common textbooks [10, 11].

2.1 Elementary Particles

Figure 2.1 shows an overview of the Standard Model of elementary particles. It is divided into three generations of matter and further into quarks and leptons. Together with the gauge bosons and the scalar Higgs boson, we have all the elementary particles.

The charge of the weak interaction is the quantum number *weak isospin*. For the left-handed[1] fermions and the corresponding right-handed antiparticles, it leads to a doublet in an abstract space with the weak isospin $I = \frac{1}{2}$ and third component $I_3 = \pm\frac{1}{2}$. The right-handed particles and left-handed antiparticles have a weak isospin $I = 0$, occur thereby in singlets and will not be described further here.

With the electric charge q and the weak isospin I, the hypercharge Y can be defined as $Y = 2(q - I_3)$ and is for leptons $Y = -1$ and for quarks $Y = +\frac{1}{3}$. Again, this is only true for left-handed particles and right-handed antiparticles.

For each generation of quarks, there is an up-type quark with an electric charge[2] of $q = +\frac{2}{3}e$ (and third component of the weak isospin $I_3 = +\frac{1}{2}$) and a down-type quark with an electric charge of $q = -\frac{1}{3}e$ (and third component of the weak isospin $I_3 = -\frac{1}{2}$). For the first generation, we have the up quark (u) and the down quark (d). For the second generation we have the charm (c) and strange quark (s) and finally for the third generation we have the top (t) and bottom quark (b). Across generations, the masses of the quarks increase.

---

[1]Where left-handed means particles with negative chirality.
[2]In units of the elementary electric charge $e = 1.602 \times 10^{-19}\,\mathrm{C}$.
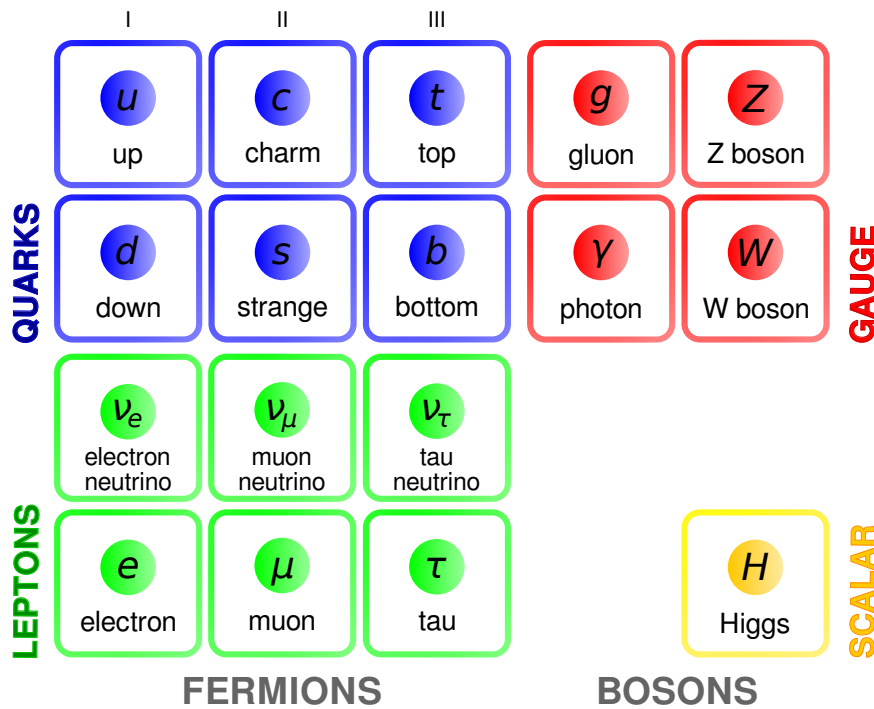
Elementary Particles of the Standard Model

Figure 2.1: Elementary particles of the Standard Model. It contains twelve particles with six quarks and six leptons (each of them has its respective antiparticle), four gauge bosons and one scalar boson – the Higgs boson.

The situation is almost the same for the three generations of leptons. Each of them has a neutrino with no electric charge (and third component of the weak isospin $I_3 = +\frac{1}{2}$) and a lepton with an electric charge $q = -e$ (and third component of the weak isospin $I_3 = -\frac{1}{2}$).

In the first generation, we have the electron neutrino (ν_e) and the electron (e^-). Then we have the muon neutrino (ν_μ) with the muon (μ^-) in the second generation and the tau neutrino (ν_τ) with the tau (τ^-) in the third generation. And again, the charged leptons become heavier across generations.

All particles that form matter are fermions and thus have a spin of $\frac{1}{2}$. Four gauge bosons with an intrinsic spin of 1 are responsible for the interaction of quarks and leptons through the three of the four known fundamental forces – gravitation is not considered in the SM. The gluon (g) is responsible for the strong force whereas the photon (γ) is the force carrier of the electromagnetic force and the Z- and $W^\pm$-bosons are the exchange particles of the weak force. Finally we have one scalar boson, the Higgs boson (H). It is the quantum exci-

tation of the Higgs field. The particles interact with that field via the Higgs boson and get mass (except for the gluon and photon) [12–17]. Neutrinos are considered massless in the SM, however, the theory of neutrino oscillations indicates that they have finite mass[3] [18].

The strong nuclear force confines quarks into hadrons. In contrast to the other three known forces, the potential of the strong force increases when the distance between two quarks is increased. Therefore, the binding energy grows and at some point it is more favourable to create a new quark-antiquark pair instead of increasing the distance any further. This phenomena is called *hadronisation* and it is responsible for quarks appearing as jets in the detector.

Table 2.1 shows an overview of the leptons, quarks, and bosons described in the SM, together with their properties. The SM can be expressed as a gauge theory with three symmetry groups [10, 11]

$$SU(3)_C \times SU(2)_L \times U(1)_Y,$$

where C stands for the colour charge of the strong interaction, L for left-handed particles and Y for the hypercharge of the electroweak interaction.

	particles	electric charge q	weak isospin I_3	hypercharge Y
quarks	$u,\ c,\ t$	$+\frac{2}{3}$	$+\frac{1}{2}$	$+\frac{1}{3}$
	$d,\ s,\ b$	$-\frac{1}{3}$	$-\frac{1}{2}$	$+\frac{1}{3}$
leptons	$\nu_e,\ \nu_\mu,\ \nu_\tau$	0	$+\frac{1}{2}$	-1
	$e,\ \mu,\ \tau$	-1	$-\frac{1}{2}$	-1
bosons	$W^\pm$	± 1	± 1	0
	$\gamma,\ Z$	0	0	0
	H	0	$-\frac{1}{2}$	$+1$

Table 2.1: Properties of the elementary particles in the Standard Model.

---

[3]The Nobel Prize in Physics 2015 was awarded jointly to Takaaki Kajita and Arthur B. McDonald "for the discovery of neutrino oscillations, which shows that neutrinos have mass".

2.2 The Top Quark

The top quark was predicted by Makoto Kobayashi and Toshihide Maskawa [19] in 1973 to explain the observed CP violation in kaon decays and was finally discovered by the CDF [20] and DØ [21] experiments at TEVATRON, FERMILAB in 1995. A combination measurement from TEVATRON and LHC for the top quark mass is given by [22]

$$m^t = 173.34 \pm 0.34 \,(\text{stat}) \pm 0.71 \,(\text{syst}) \text{ GeV}.$$

This mass is in the order of heavy atoms, about the same mass as the nucleus of Tungsten. The top quark has an electric charge of $+\frac{2}{3}e$ and a spin of $\frac{1}{2}$.
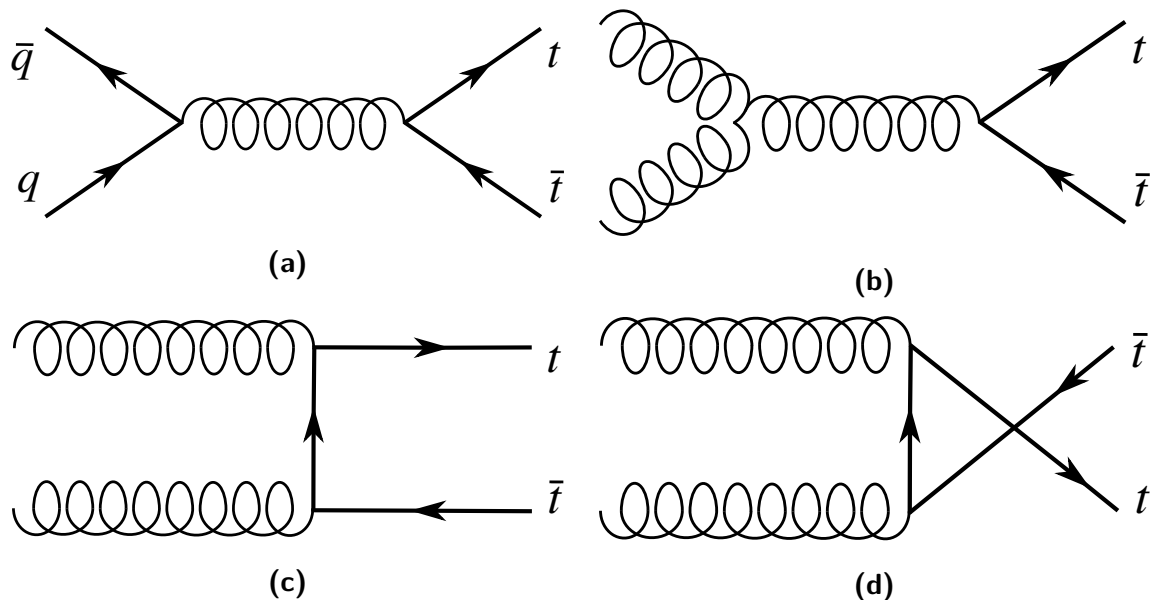

Figure 2.2: The leading order Feynman diagrams for the production of top quark-antiquark pairs. One can distinguish between quark-antiquark annihiliation (a) and gluon fusion (b) – (d).

In this section, the focus is on the production of the $t\bar{t}$ pair, as it takes place at the Large Hadron Collider (LHC). The electroweak single top quark production [22, 23] will not be discussed here. However, it was observed first at the CDF [24] and DØ [25] experiments at the TEVATRON, FERMILAB in 2009.

The leading order Feynman diagrams can be found in Figure 2.2. Figure 2.2a shows the $t\bar{t}$ production via quark-antiquark annihilation and Figure 2.2b to 2.2d shows the production via gluon fusion. It is the dominating production mode at the LHC, as the $q\bar{q}$ process requires an antiquark, and the LHC is a proton-proton collider.

Due to the very short lifetime $\tau \approx 10^{-25}\,$s, the top quark decays before hadronisation. It decays almost exclusively (99 %) to a W-boson and a b-quark and this vertex is called the Wtb vertex. The W-boson will decay further into a quark-antiquark pair or a charged lepton with its corresponding neutrino. Depending on this decay topology, one can distinguish between different decay channels. The different branching ratios for these channels are shown in Figure 2.3.
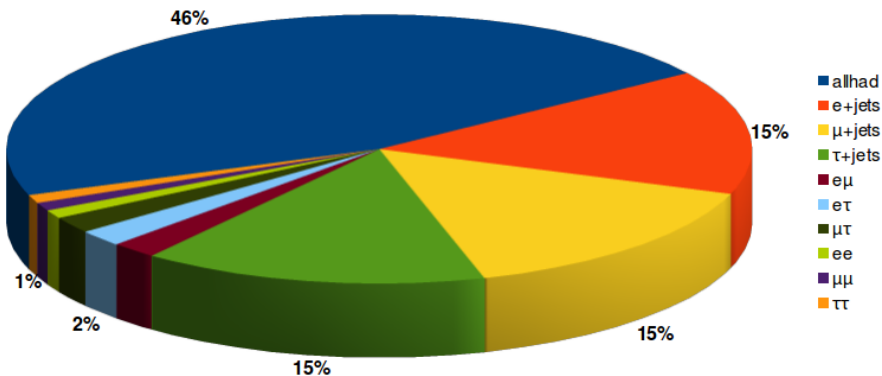

Figure 2.3: Different decay channels for $t\bar{t}$ with their respective branching ratios.

If both W-bosons from the top and antitop quark decay into quarks, this is called the all-hadronic channel and has six jets in the final state. If only one W-boson decays into quarks and the other into leptons, this channel is called the ℓ+jets channel. Depending on the final state lepton, it is further classified into e+jets or μ+jets. Due to the lepton universality of the weak interaction, the branching ratio for decays into each lepton is the same.

The case of τ+jets is not considered here, because the τ decays further into either lighter leptons or hadronically into pions or kaons with various branching ratios. As it will be mentioned in Section 3.2.1, there is no τ detector within ATLAS. So they will be detected as jets, electrons, or muons.

The last possible decay topology is the dileptonic case, when both W-bosons decay leptonically. So the $t\bar{t}$ decay topology can be divided in three channels: all hadronic, ℓ+jets, and dileptonic. The Feynman diagram of the dilepton decay can be found in Figure 2.4. This dileptonic channel shows a very clear signature in the detector signal, because only
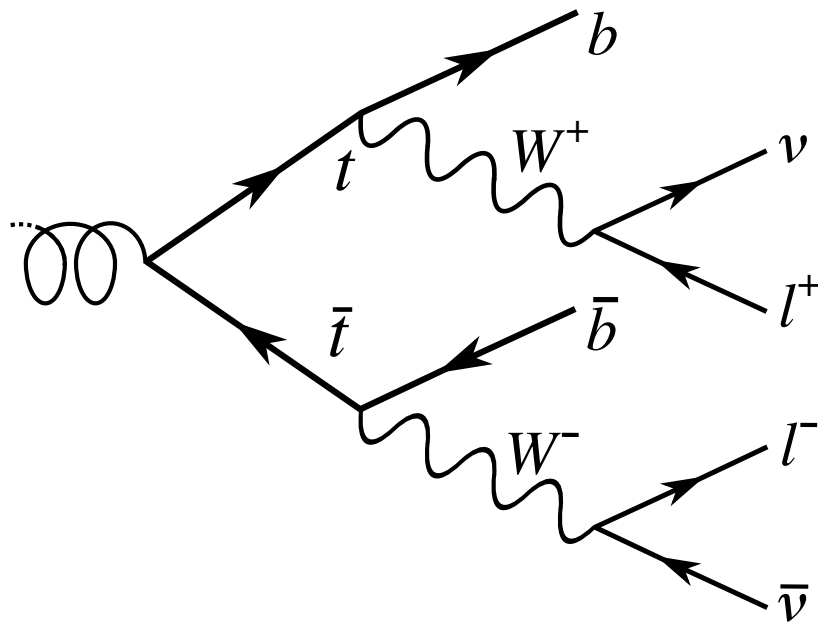
Figure 2.4: Feynman diagram of one possible decay topology of the top quark-antiquark pair into the dileptonic channel. The final lepton (ℓ) will either be an electron or a muon with its corresponding neutrino. The b-quarks will be detected as jets in the detector.

two jets will appear in the final state. The leptons can be assigned to the originating top via their charge. Thus, only two possible permutations of the jets are possible in order to find the right assignment to reconstruct the top quark kinematics.

The main background of the $t\bar{t}$ dilepton channel is the Wt process. This is a single top quark production with a W-boson, written as

$$b + g \rightarrow W^- + t.$$

The top quark will again decay into a b-quark and a W-boson. If then both W-bosons decay leptonically, this final state contains two neutrinos and two charged leptons with one jet. Therefore, it shows a similar signature to the $t\bar{t}$ dilepton channel in the detector.

3 Experimental Setup

To establish a common European organisation for nuclear research, the *Conseil européen pour la recherche nucléaire* (CERN) was founded in Geneva, Switzerland in 1954. It consists of 22 member states and is the largest particle physics research centre in the world.

3.1 The Large Hadron Collider

The largest and most powerful particle accelerator, the Large Hadron Collider (LHC), is located at CERN [26]. It has a circumference of about 27 km and lies in a tunnel approximately 100 m beneath the ground. It can either be used for proton or heavy ion acceleration. The first collisions took place in March 2010 at a centre-of-mass energy of $\sqrt{s} = 7$ TeV. In 2012 it was increased to 8 TeV. This period is called Run I.

After that, the LHC was shut down for about two years in order to repair and exchange magnets and prepare it for the next run – Run II. Since 2015 the LHC is running at $\sqrt{s} = 13$ TeV, a significant increase compared to the first three years of the LHC Run I. In $2019 - 2020$ another long shut down is scheduled to perform the next upgrade. In 2021 for Run III, it is planned to have $\sqrt{s} = 14$ TeV.

A schematic representation of the accelerator is shown in Figure 3.1. Before injecting the protons to the LHC in bunches, various preaccelerators are used. First, a linear accelerator (LINAC 2) accelerates the protons, which are obtained by stripping the electrons from the hydrogen, to the Proton Synchrotron Booster (PSB).

After passing the Proton Synchrotron (PS) and the Super Proton Synchrotron (SPS), each bunch of protons has an energy of 450 GeV and is injected into the LHC, where they will be accelerated further. The two beams are accelerated in two pipes in the opposite direction. Interactions between those two beams take place every 25 ns leading to a bunch collision rate of 40 MHz.
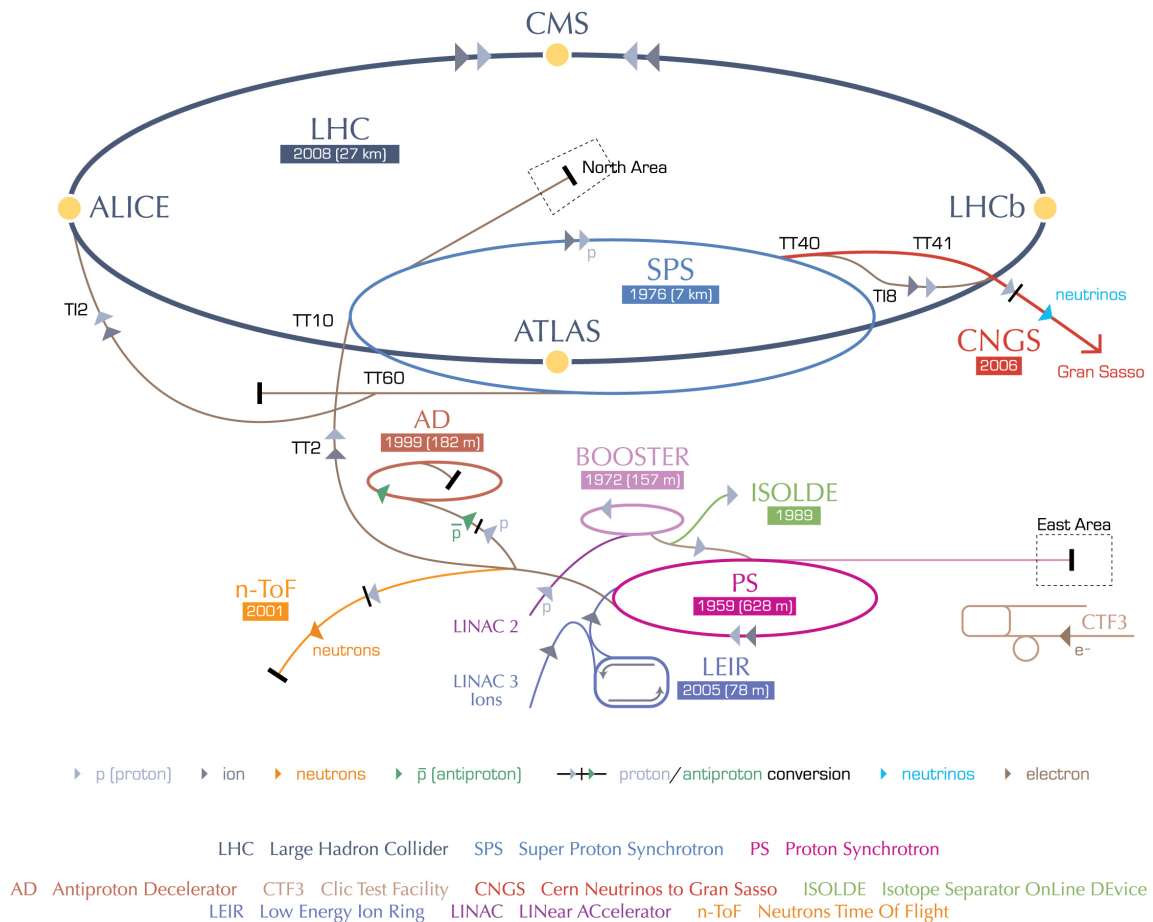
Figure 3.1: Schematic representation of the acceleration complex. © Cern

Experiments The four main experiments are placed at the four intersection points of the LHC, namely Atlas [27], CMS [28], LHCb [29], and Alice [30]. Also three minor detectors are located there, sharing these intersection points with the larger ones. They are called LHCf [31], TOTEM [32] and MoEDAL [33], which will not be discussed here. Nevertheless they are worth mentioning.

A major goal of one of the four large experiments Alice is searching for quark-gluon plasma that existed shortly after the Big Bang. Another experiment, the LHCb is searching for the asymmetry between matter and antimatter. The two large general-purpose detectors CMS and Atlas are constructed for similar measurements and their main focus lies on studies of the Higgs boson as well as searches for new physics. This thesis uses Monte Carlo simulations to generate events that are further simulated to have Atlas detector effects on them. The Atlas experiment will be described in the following section.
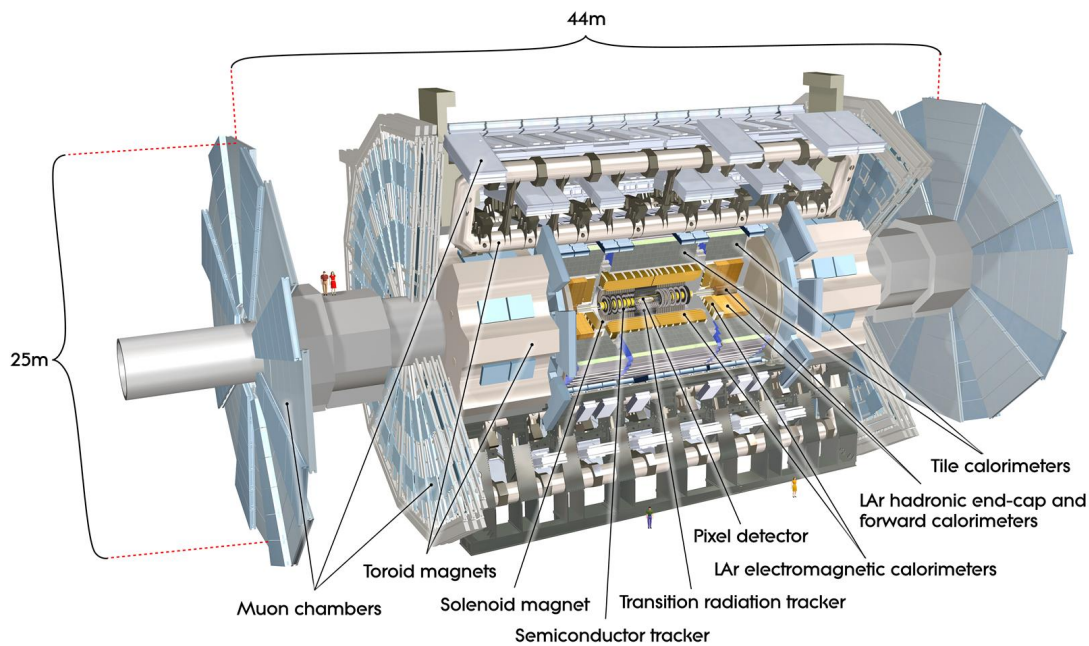
Figure 3.2: Schematic representation of the ATLAS detector. © CERN

3.2 The ATLAS Experiment

The ATLAS Collaboration is a union of over 3 000 scientific authors from 182 institutions in 38 countries around the world and is one of the biggest scientific collaborations.
The ATLAS detector is 44 m long and 25 m in diameter with a mass of 7 000 tonnes. It is an air core toroidal detector with sub-detectors that are arranged in an onion-like pattern forming a cylindrical shape. Figure 3.2 shows a schematic picture of the detector.

3.2.1 Detector Setup

The *Inner Detector* (ID) of ATLAS contains three different sensors (Pixel Detector, Semiconductor Tracker, and Transition Radiation Tracker) to measure the direction, momentum, and charge of the particles. This Inner Detector extends to a radius of almost 1.2 m and is surrounded by an external magnetic field of 2 T parallel to the beam axis.
Moving from the centre to the outer region, the next parts of the ATLAS detector are the *Calorimeters*. They measure the total energy of the particle and therefore absorb all the kinetic energy and stop it entirely. There are electromagnetic calorimeters for the interactions with electrons and photons, and hadronic calorimeters for the interaction of hadrons. The calorimeters are sub-divided into the Liquid Argon Calorimeter and the Tile Hadronic Calorimeter.

The third main part of the detector is the *Muon Spectrometer*. Normally, all muons pass through the first two parts undetected, due to the weak interaction of muons with matter. Hence, the large Muon Spectrometer measures and detects the momentum and energy of the muons. It contains four different subsections, Thin Gap Chambers, Resistive Plate Chambers, Monitored Drift Tubes and Cathode Strip Chambers [27].

3.2.2 Coordinate System

The ATLAS detector uses a right-handed coordinate system, with the x-axis pointing towards the centre of the main accelerator ring, the y-axis upwards and the z-axis along the beam. The angle φ is in the x-y-plane, and between the z-axis and the particle in the detector is the polar angle ϑ. Instead of using this angle, an often chosen quantity is the pseudorapidity defined as

$$\eta = -\ln\left[\tan\left(\frac{\vartheta}{2}\right)\right].\tag{3.1}$$

The distance between two particles within the detector is then defined as

$$\Delta R = \sqrt{(\Delta\varphi)^2 + (\Delta\eta)^2}.\tag{3.2}$$

The momentum p_T and energy E_T in the transverse plane perpendicular to the beam axis are defined as

$$p_T = \sqrt{p_x^2 + p_y^2} \qquad \text{and} \qquad E_T = \sqrt{p_T^2 + m^2},\tag{3.3}$$

where p_x is the momentum in the x-direction, p_y in the y-direction, and m denotes the invariant mass.

3.2.3 Monte Carlo Samples

For this thesis, only Monte Carlo (MC) generated samples are used. They are generated taking into account next-to-leading order effects. For the signal ($t\bar{t}$ dileptonic events), the event generator POWHEG+PYTHIA8 [34, 35], whereas for the background (Wt inclusive events), the event generator POWHEG+PYTHIA6 [34, 36] is used. For the signal, the generated sample contains about 40 million simulated events whereas for the background, the sample has about 10 million simulated events.

4 Reconstruction of t$\bar{\text{t}}$ Dileptonic Events

In the final state of a $t\bar{t}$ dileptonic event, as shown in Figure 2.4, there are two jets originating from the two b-quarks, two leptons with opposite charges sign and two neutrinos. Considering the four-momenta of all the six particles, there are 24 parameters, which need to be solved.

The four-momenta of the jets (p^b) and charged leptons (p^ℓ) can be measured in the detector. Moreover, the masses of all six particles are known. In addition, the momentum of the two neutrinos in the x- and y-direction are measured as missing transverse energy E_x^{miss} and E_y^{miss}. This reduces the degrees of freedom of the system to six free parameters, which need to be determined. Thus, more constraints are required.

4.1 The Kinematic Reconstruction of t$\bar{\text{t}}$ Events

The first constraint can be applied by kinematic considerations for the masses of different particles, which will decay further and therefore not appear in the final state.

The invariant masses of both W-bosons have to be the same as the absolute value of the four-momentum vectors of the decay products. This means

$$m^{W2} = \left(p^\ell + p^\nu\right)^2,\tag{4.1}$$

where the four-momentum of the neutrino is denoted as p^ν. The same argument holds for both top quarks, where we also assume the equality of the masses of top and antitop quark

$$m^{t2} = \left(p^\ell + p^\nu + p^b\right)^2.\tag{4.2}$$

Furthermore, we know the mass of the W-boson $m^W = 80.4\,\text{GeV}$ and the mass of the b-quark $m^b = 4.3\,\text{GeV}$ [22]. The mass of the top quark m^t is also known, and can either be fixed to a certain value or smeared over a range within the resolution. Moreover, the invariant mass of the lepton is negligible compared to the other particles and can therefore be set to $m^\ell \approx 0\,\text{GeV}$.

From Equation (4.1) we can derive

$$m^{W\,2} = \left(E^l + E^\nu\right)^2 - \left(\vec{p}^{\,l} + \vec{p}^{\,\nu}\right)^2 = 2\left(E^l E^\nu - \vec{p}^{\,l}\vec{p}^{\,\nu}\right)$$

$$\Rightarrow \quad E^\nu = |\vec{p}^{\,\nu}| = \frac{1}{E^l}\left(\frac{m^{W\,2}}{2} + \vec{p}^{\,l}\vec{p}^{\,\nu}\right). \tag{4.3}$$

Similarly for Equation (4.2), we get

$$m^{t\,2} = \left(E^l + E^\nu + E^b\right)^2 - \left(\vec{p}^{\,l} + \vec{p}^{\,\nu} + \vec{p}^{\,b}\right)^2$$

$$= m^{W\,2} + m^{b\,2} + 2\left(E^l E^b + E^\nu E^b - \vec{p}^{\,l}\vec{p}^{\,b} - \vec{p}^{\,\nu}\vec{p}^{\,b}\right)$$

$$\Leftrightarrow \quad E^\nu = |\vec{p}^{\,\nu}| = \frac{m^{t\,2} - m^{W\,2} - m^{b\,2} - 2p^l p^b}{2E^b} + \frac{\vec{p}^{\,\nu}\vec{p}^{\,b}}{E^b} \tag{4.4}$$

To boost into the neutrino rest frame along the beam axis with $p_z^\nu = 0\,\text{GeV}$, we apply the Lorentz transformation

$$L = \begin{pmatrix} \cosh(\eta^\nu) & 0 & 0 & -\sinh(\eta^\nu) \\ 0 & 1 & 0 & 0 \\ 0 & 0 & 1 & 0 \\ -\sinh(\eta^\nu) & 0 & 0 & \cosh(\eta^\nu) \end{pmatrix} \tag{4.5}$$

to Equations (4.3) and (4.4). This yields

$$p_T^\nu = \frac{m^{W\,2}}{2E^{l'}} + \frac{p_x^l p_x^\nu}{E^{l'}} + \frac{p_y^l p_y^\nu}{E^{l'}} \tag{4.6}$$

$$p_T^\nu = \frac{m^{t\,2} - m^{W\,2} - m^{b\,2} - 2p^l p^b}{2E^{b'}} + \frac{p_x^\nu p_x^b + p_y^\nu p_y^b}{E^{b'}} \tag{4.7}$$

where $E^{l'} = E^l\cosh(\eta^\nu) - p_z^l\sinh(\eta^\nu)$ and $E^{b'} = E^b\cosh(\eta^\nu) - p_z^b\sinh(\eta^\nu)$. Comparing p_T^ν in Equation (4.6) and (4.7), and solving for p_x^ν gives a linear equation for the neutrino momentum in the x-direction $p_x^\nu = a \cdot p_y^\nu + b$ with constants

$$a = \frac{p_y^l E^{b'} - p_y^b E^{l'}}{p_x^b E^{l'} - p_x^l E^{b'}}, \tag{4.8}$$

$$b = \frac{E^{l'}\left(m^{t\,2} - m^{W\,2} - m^{b\,2} - 2p^l p^b\right) - E^{b'} m^{W\,2}}{2\left(p_x^l E^{b'} - p_x^b E^{l'}\right)}. \tag{4.9}$$

Using the definition of p_T given in Equation (3.3) and eliminating p_x^ν in Equation (4.6), one obtains

$$\sqrt{(a^2+1)(p_y^\nu)^2 + 2ab\,p_y^\nu + b^2} = \frac{m^{W2}}{2E^{l\prime}} + \frac{p_x^l}{E^{l\prime}}(a p_y^\nu + b) + \frac{p_y^l}{E^{l\prime}} p_y^\nu \qquad (4.10)$$

Solving Equation (4.10) for the neutrino momentum p_y^ν in the y-direction leads to a quadratic equation $c(p_y^\nu)^2 + d p_y^\nu + f = 0$ with constants

$$c = a^2 + 1 - \left(\frac{p_x^l}{E^{l\prime}}\, a + \frac{p_y^l}{E^{l\prime}} \right)^2 , \qquad (4.11)$$

$$d = 2ab - 2 \left(\frac{m^{W2}}{2E^{l\prime} + \frac{p_x^l}{E^{l\prime}} b} \right) \cdot \left(\frac{p_x^l}{E^{l\prime}}\, a + \frac{p_y^l}{E^{l\prime}} \right) , \qquad (4.12)$$

$$f = b^2 - \left(\frac{m^{W2}}{2E^{l\prime} + \frac{p_x^l}{E^{l\prime}} b} \right)^2 . \qquad (4.13)$$

Thus, the solution is given by

$$p_{y_\pm}^\nu = -\frac{d}{2c} \pm \frac{1}{2c} \sqrt{d^2 - 4cf}. \qquad (4.14)$$

The linear equation for $p_x^\nu = a \cdot p_y^\nu + b$ can be used to calculate the momentum of the neutrino in the x-direction, and the momentum along the beam axis can be determined by using $p_z^\nu = p_T^\nu \sinh \eta^\nu$. For the neutrino and the antineutrino, there are up to two solutions per neutrino. So for each dilepton event, there arises an up to fourfold ambiguity for the reconstructed four-momenta of the neutrinos, which needs to be solved.

The so-called Neutrino Weighting Method uses these calculations for the reconstruction of the $t\bar{t}$ dilepton event and it will be discussed in the following section.

4.2 Neutrino Weighting Method

The *Neutrino Weighting Method* [37, 38] was originally developed by the DØ collaboration as a reconstruction algorithm of the $t\bar{t}$ dileptonic event for the top mass measurement. This algorithm ignores first the constraints of the missing energy in the x- and y-direction, E_x^{miss} and E_y^{miss}, but it adds three other assumptions in order to solve the under-constrained system as discussed in Section 4.1.

The first additional assumption is the known top quark mass. As one can see in Equation (4.4) the top quark mass has been set as an additional parameter to solve the equation.

Another assumption is the distribution of the neutrino and antineutrino pseudorapidity η, in order to apply the Lorentz boost into the neutrino p_z rest frame. In inclusive QCD, the SM predicts a rectangular pseudorapidity distribution, but due to detector resolution and higher order effects, it is expected to be a smeared function and can be modelled by a Gaussian distribution with mean value $\mu = 0$ and standard deviation σ.

Now, the system is fully constrained and can be solved as described in the calculation in Section 4.1. Due to the quadratic Equation (4.14), there remain up to four possible solutions for the neutrino momenta. For each of these solutions, the expected missing transverse energy

$$E_{x|y,\text{exp}}^{\text{miss}} = p_{x|y}^{\nu} + p_{x|y}^{\bar{\nu}} \tag{4.15}$$

is calculated and compared to the observed $E_{x|y,\text{obs}}^{\text{miss}}$, since these two constraints are no longer included in the calculations. Thus, for each event a weight w is defined as

$$w = \sum_{i=1}^{N} \exp\left(-\frac{1}{2}\left[\frac{E_{x,\text{exp},i}^{\text{miss}} - E_{x,\text{obs}}^{\text{miss}}}{\sigma_{E_x^{\text{miss}}}}\right]^2\right) \cdot \exp\left(-\frac{1}{2}\left[\frac{E_{y,\text{exp},i}^{\text{miss}} - E_{y,\text{obs}}^{\text{miss}}}{\sigma_{E_y^{\text{miss}}}}\right]^2\right), \tag{4.16}$$

where $\sigma_{E_x^{\text{miss}}}$ and $\sigma_{E_y^{\text{miss}}}$ are the missing energy resolution in the x- and y-direction, respectively. Here, i runs over all possible assumptions of jet assignments and pseudorapidity distributions. The detector resolution is taken into account by allowing the kinematics of leptons and jets to fluctuate within a certain range according to their resolution. This leads to an assumed top quark mass. For each of these smeared events, the weights are summed together. Therefore, we have a weight distribution for different top quark mass assumptions, which indicates how well the top quark mass matches the reconstructed event.

The neutrinos remain unsolved, because the fourfold ambiguity in the reconstruction is still there. This thesis focuses on the weights defined in Equation (4.16) and how one can use that to choose the correctly reconstructed neutrino.

4.3 Kinematic Likelihood Fitter

The *Kinematic Likelihood Fitter* (KLFitter) [39] is a framework written in `C++` based on a likelihood approach for the kinematic reconstruction of the $t\bar{t}$ event. The framework is independent of the physics processes and in particular independent of the experiment. Therefore, it can be used for various top quark analysis. It included initially the algorithm for the reconstruction of the ℓ+jets channel, but has been updated to reconstruct various

$t\bar{t}$ decay channels, i.a. the dileptonic channel. The algorithm finds the best permutation of the association of particles to the detected jets by maximizing a likelihood function.

For the dileptonic $t\bar{t}$ final state, the likelihood $\mathcal{L}$ is given by [40]

$$
\begin{aligned}
\mathcal{L} = &\left(\prod_{\xi=x,y} G\left(E_{\xi,\mathrm{obs}}^{\mathrm{miss}} \,\Big|\, p_\xi^\nu, p_\xi^{\bar{\nu}}, \sigma_{E_\xi^{\mathrm{miss}}}\left(m_t,\, m_W,\, \eta^\nu,\, \eta^{\bar{\nu}}\right) \right) \right) \cdot \\
&G\left(\eta^\nu|m^t\right) \cdot G\left(\eta^{\bar{\nu}}|m^t\right) \cdot W\left(\tilde{E}_{\mathrm{jet}_1}|E_{b_1}\right) \cdot W\left(\tilde{E}_{\mathrm{jet}_2}|E_{b_2}\right) \cdot \\
&W\left(\tilde{\varepsilon}_1|\varepsilon_1\right) \cdot W\left(\tilde{\varepsilon}_2|\varepsilon_2\right) \cdot \Big(m(\ell_1,\,\mathrm{jet}_1) + m(\ell_2,\,\mathrm{jet}_2)\Big)^\alpha.
\end{aligned}
\tag{4.17}
$$

The likelihood consists of different terms with different meanings.

Neutrino Weighting   The first line with the product of the Gaussian functions G compares the expected missing transverse energy $E_{\xi,\mathrm{exp}}^{\mathrm{miss}} = p_\xi^\nu + p_\xi^{\bar{\nu}}$ with the observed $E_{\xi,\mathrm{obs}}^{\mathrm{miss}}$ in the x- and y-direction ($\xi = x, y$). This term originates from the Neutrino Weighting Method in Equation (4.16) and takes also the detector resolution $\sigma_{E_\xi^{\mathrm{miss}}}$ into account. The other two Gaussian functions are the predicted pseudorapidities of the neutrino and antineutrino which could also depend on the top quark mass m^t.

Transfer Functions   The transfer functions W describe higher order effects and detector resolutions. This terminates in an energy difference between the reconstructed objects after calibration $\tilde{E}$ and leading order parton-level energy E. In case of electrons, the transfer functions are indeed given by the energy, whereas in the case of muons, the terms are given by the transverse momentum p_T. To distinguish between the ee, $e\mu$, and $\mu\mu$ subchannel, this results in $\varepsilon = E_\ell$ for electrons and $\varepsilon = p_{T_\ell}$ for muons.

Additional term   The last "additional term" is introduced leading to a better reconstruction efficiency. The invariant mass of a correctly assigned lepton plus jet to the originated top (or antitop) quark is expected to be smaller compared to the case of a wrong assignment. To increase the likelihood, and therefore the efficiency, the tuning parameter α has to be negative. It is found, that the best separation for the correct assignment to the top and antitop quark is provided by $\alpha = -2$ [40].

For the $t\bar{t}$ dilepton final state, there are two possible permutations due to the correct assignment of the jets to the top or antitop quark. The positively charged lepton is assigned to the top quark and the negatively charged lepton is assigned to the antitop quark, as one can see in Figure 2.4.

5 Results

The ATHENA framework [41] is used throughout this analysis. It provides all the necessary tools for research on top quark physics within ATLAS.

All the studies made in this chapter are based on the *reconstruction level* after the event selection described in the following section and running the ATHENA framework. They will be compared to the MC *truth level* to calculate distributions like ΔR between true and reconstructed particles as defined in Equation (3.2).

Since the final state of the $t\bar{t}$ dilepton event always contains a neutrino and an antineutrino, each analysis is performed for both particles. Mostly the variation between them is negligible and therefore only the neutrino is considered. If it is important to show both distributions, this is mentioned specially. Furthermore, all histograms and graphs are normalised to 1, if not stated otherwise.

5.1 Event Selection

As shown in Figure 2.3, only a small fraction ($\approx 6\,\%$) of $t\bar{t}$ events decay into the dileptonic channel. In addition, leptons and jets can only be detected if their energy is above a certain threshold and their position in a certain η region, due to the beam pipe and the calibration of the sensors in the detector. Therefore, various cuts on the full Monte Carlo samples (see Section 3.2.3) are necessary.

According to the different subchannels ee, $e\mu$, or $\mu\mu$, exactly two oppositely charged leptons are required. Furthermore, for each of the leptons and jets, a transverse momentum $p_T > 25\,\mathrm{GeV}$ is required. Moreover, there have to be at least two b-tagged jets, i.e. at least two jets in the detector were assigned and tagged to come from a b-quark. The b-tagging [42] is done at a working point of $60\,\%$ efficiency.

This leads to 576 318 selected events in the signal sample and 5356 selected events in the background sample.

5.2 Neutrino Pseudorapidity Distribution

As shown in the calculations for the neutrino reconstruction in Section 4.1, two of the additional assumptions are related to the neutrino and antineutrino pseudorapidity distributions. These distributions are predicted by the Standard Model, with higher order effects and detector resolution taken into account, they can be approximated by a Gaussian distribution. Moreover, it is also expected that there is no difference between the neutrino and antineutrino. Thus, both distributions can be modelled by one function.

Due to the different detection methods (see Section 3.2.1), branching ratios (see in Figure 2.3), and applied cuts on the MC sample, one has to distinguish between the different final leptons ee, $e\mu$, and $\mu\mu$ in the event. For each of these subchannels, the pseudorapidity truth distributions are plotted and fitted via a Gaussian function

$$g(x) = \frac{1}{\sqrt{2\pi}\,\sigma} \, \exp\left(-\frac{1}{2}\left[\frac{x-\mu}{\sigma}\right]^2\right).$$

To facilitate an optimal fit, one sets the mean value $\mu = 0$, as it is predicted from the Standard Model, and allows only the standard deviation σ to vary. The optimal reduced $\chi_r^2 = \chi^2/\text{NDF}$ is found for a binning of 1000 bins in the histogram, where NDF is the number of degrees of freedom in the fit.

This fit was already done for $\sqrt{s} = 8\,\text{TeV}$ and is currently implemented in KLFitter. Due to the higher available energy of $13\,\text{TeV}$ and detector upgrades, the pseudorapidity distribution needs to be updated.

In the past, the standard deviation σ of the Gaussian g weakly depended on the top mass m^t with two additional parameters n, k via $\sigma = n \cdot m^t + k$. For this thesis, only an MC sample with one fixed top mass is available. Consequently, the additional freedom of two parameters is no longer meaningful and the fit is done by only one free parameter σ.

The fitted neutrino and antineutrino distributions can be found in Figure 5.1, separated into the different categories based on the leptons in the final state.

A comparison between the current σ values at $8\,\text{TeV}$ and the new fitted ones at $13\,\text{TeV}$ can be found in Table 5.1. As one expects, the new pseudorapidity distribution at the higher centre-of-mass energy has a larger standard deviation σ and is therefore broader compared to the old one at lower energy. This is compatible with the predictions, because the events, when the neutrino is radiated perpendicular to the beam axis, namely $\eta = 0$, happen less at higher energy. It is thereby more favourable for the neutrino to leave the system under a larger modulus of η, which means a smaller angle to the beam pipe.
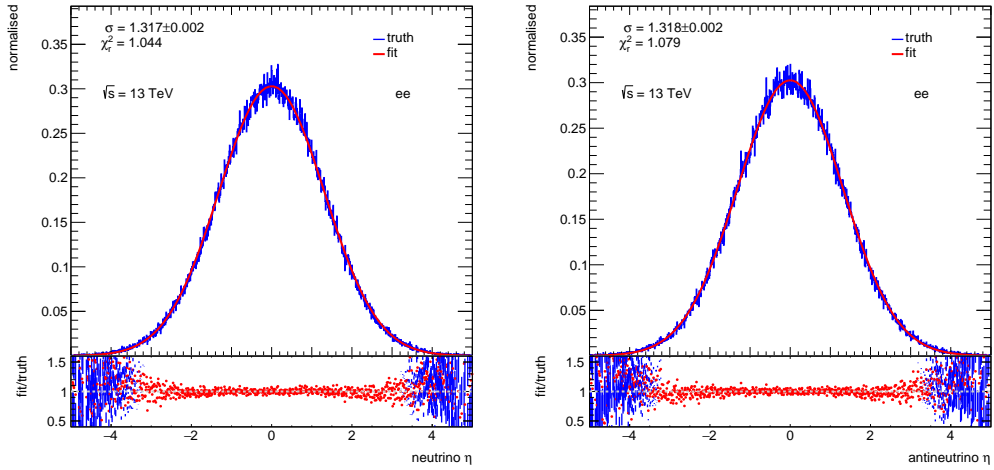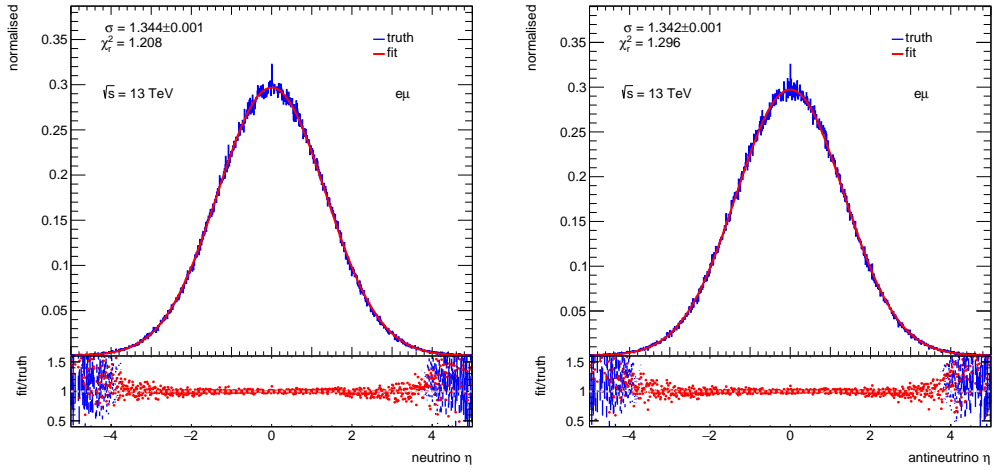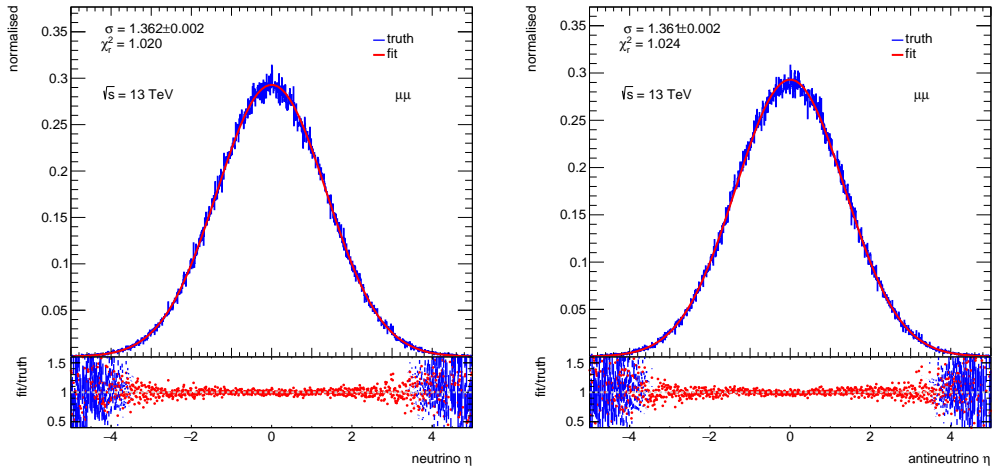
(a) Neutrino (left) and antineutrino (right) η distribution in the *ee* channel.

(b) Neutrino (left) and antineutrino (right) η distribution in the *eµ* channel.

(c) Neutrino (left) and antineutrino (right) η distribution in the *µµ* channel.

Figure 5.1: Gaussian fit to the neutrino pseudorapidity truth distribution with 1000 bins in the (a) *ee* channel, (b) *eµ* channel, and (c) *µµ* channel. The reduced χ^2_r is close to 1.

channel	σ_{fit} (13 TeV)	σ_{old} (8 TeV)
ee	1.318	1.166
eμ	1.343	1.291
μμ	1.362	1.226

Table 5.1: Comparison between the fitted Gaussian standard deviation σ for $\sqrt{s} = 13$ TeV and $\sqrt{s} = 8$ TeV. For the fitted values, the arithmetic mean of neutrino and antineutrino was calculated.

5.3 Reconstruction of the $t\bar{t}$ Event

With these updated pseudorapidity distributions, the reconstruction of the neutrino and hence the full reconstruction of the $t\bar{t}$ event can be done. For that, the calculations described in Section 4.1 are executed for each event. Due to the quadratic nature of Equation (4.14), different cases have to be considered:

1. If the term under the square root is negative, there is no real solution for that neutrino in the given event. Hence, the reconstruction fails and this event cannot be considered for the performance studies. This will be discussed further in Section 5.3.2, specifically how often this happens and its mitigation.

2. If there is exactly one solution, this means the term under the square root is equal to zero, the neutrino is reconstructed unambiguously. However, this happens only for one single event in the analysis.

3. Most often, the reconstruction leads to two solutions for the momentum p_x^ν and p_y^ν for each neutrino. So for the full $t\bar{t}$ event with two neutrinos, there is a fourfold ambiguity, even if the jet assignment is determined correctly. This still needs to be solved and will be discussed further in Section 5.3.2.

5.3.1 Matching Efficiencies

A reconstructed particle is called *matched* to the truth particle, if it lies within a certain ΔR of truth. The lepton in the final state is considered matched if it lies within $\Delta R < 0.1$ to the truth lepton and the *b*-jet is considered matched, if it lies within $\Delta R < 0.3$ to the truth *b*-quark. The assignment of the *b*-jet to the top or antitop quark is given by KL-Fitter. Due to additional radiation or pile-up, the $t\bar{t}$ dileptonic event can have more than two jets. Therefore, the jet-parton assignment with the highest likelihood value within KLFitter is chosen to be the correctly assigned one.

For the reconstructed *b*-jet, as well as for the lepton, two different approaches are possible. One can either use the particle on reconstruction level (referred as *reco* in the following), which is reconstructed by the detector. Or one uses the particles that passed KLFitter with transfer functions and additional assumptions, as mentioned in Section 4.3, were taken into account (referred as *fit* in the following). However, for the reconstruction matching efficiencies, there is no difference between them.

The matching efficiencies were determined for different combinations: If both *b*-jets match the two true *b*-quarks, if only the *b*-quark or the $\bar{b}$-quark is matched by the *b*-jet and if at least one *b*-jet matches either the *b*- or $\bar{b}$-quark. Finally, also the matching efficiency for both charged leptons were calculated. Furthermore, the efficiencies were separated into the different decay channels *ee*, *eμ*, and *μμ*. The obtained values are shown in Table 5.2.

channel	*ee*	*eμ*	*μμ*
both *b*-jets	65.5 %	66.4 %	67.4 %
b-jet	73.0 %	73.6 %	74.6 %
$\bar{b}$-jet	73.1 %	73.6 %	74.7 %
at least 1 *b*-jet	80.5 %	80.9 %	81.9 %
both leptons	97.6 %	98.4 %	98.7 %

Table 5.2: Reconstruction matching efficiencies for different decay channels *ee*, *eμ*, and *μμ*. Both leptons are considered matched if $\Delta R < 0.1$ and each *b*-jet if $\Delta R < 0.3$.

The transverse momentum of the *b*-quark is shown in Figure 5.2. The distributions for the fitted (from KLFitter with transfer function, containing the detector resolution) and reconstructed (without transfer functions) values are compared. As one expects, the fitted distribution is closer to the truth one, due to the inclusion of transfer functions.

5.3.2 Performance

In cases where the KLFitter algorithm does not find the best permutation (as mentioned in Section 4.3), the likelihood cannot be maximised. Then, no fitted values are in the KLFitter output and therefore no reconstruction can be executed. This happens in about 0.9 % of cases, and these events are excluded in the following analysis.

As mentioned in Section 5.3, different cases have to be considered. If there is no real solution to the quadratic equation of the neutrino momentum, the $t\bar{t}$ system cannot be reconstructed. This happens in approximately 36 % of the total events, when the detector
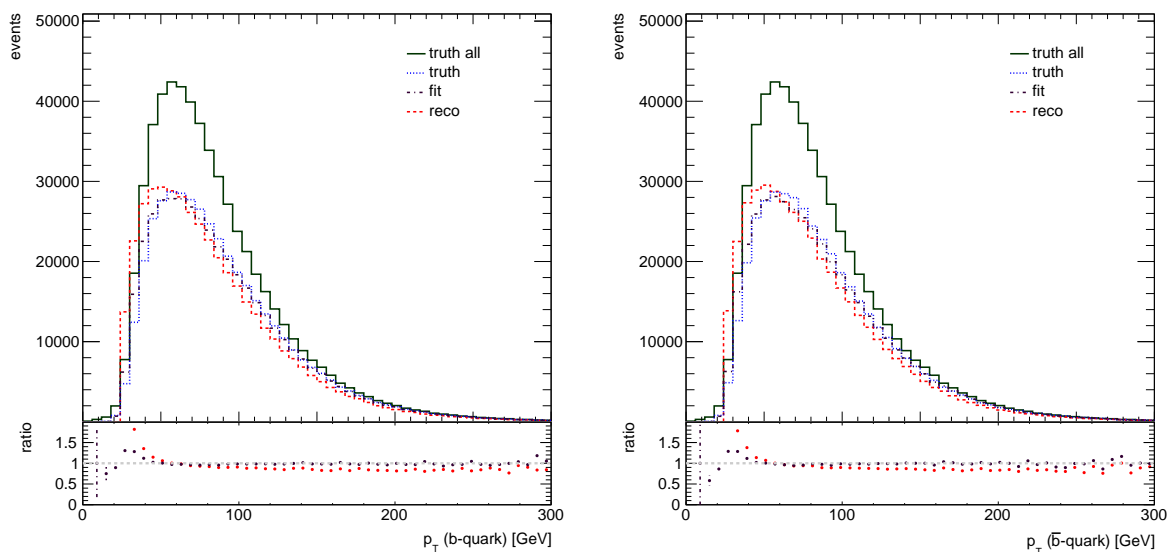
Figure 5.2: Transverse momentum of the *b*-quark on the left and $\bar{b}$-quark on the right. All truth events are shown in green, indicated by *truth all*. Only the truth events, that were matched by the *reco* (red) or *fit* (purple) values are shown in blue. The ratio of the green and the blue curve would be the reconstruction matching efficiency, as shown in Table 5.2 (for *b*- and $\bar{b}$-jet). The bottom plot shows the ratio between the fitted and reconstructed distribution to the truth one in blue.

reconstructed values are used, and in 26 % of the events for the KLFitter reconstructed objects. This needs to be optimised. Further discussion regarding this issue can be found in Section 5.4. The case of exactly one solution is trivial and also happens just for one single event.

However, in the case of two solutions for every neutrino, which happens in 64 % of the events for reco and 74 % for fitted values, the ambiguity in choosing the correct value remains. This is finally solved by taking the solution with the *highest* weight for each neutrino, where the weight w is defined as

$$w = \exp\left(-\frac{1}{2}\left[\frac{E_{x,\mathrm{exp}}^{\mathrm{miss}} - E_{x,\mathrm{obs}}^{\mathrm{miss}}}{\sigma_{E_x^{\mathrm{miss}}}}\right]^2\right) \cdot \exp\left(-\frac{1}{2}\left[\frac{E_{y,\mathrm{exp}}^{\mathrm{miss}} - E_{y,\mathrm{obs}}^{\mathrm{miss}}}{\sigma_{E_y^{\mathrm{miss}}}}\right]^2\right). \tag{5.1}$$

In contrast to Equation (4.16), it is not summed over all possible permutations, but by just computing the weight once for each neutrino solution. Then the neutrino and antineutrino with the highest weight are kept as the correctly reconstructed ones.

A physical explanation for taking only the highest weight can be given by the fact, that a larger weight corresponds to a smaller difference in the observed and expected missing transverse energy. A weight of $w = 1$ would mean that the total E_T^{miss} is assigned to the
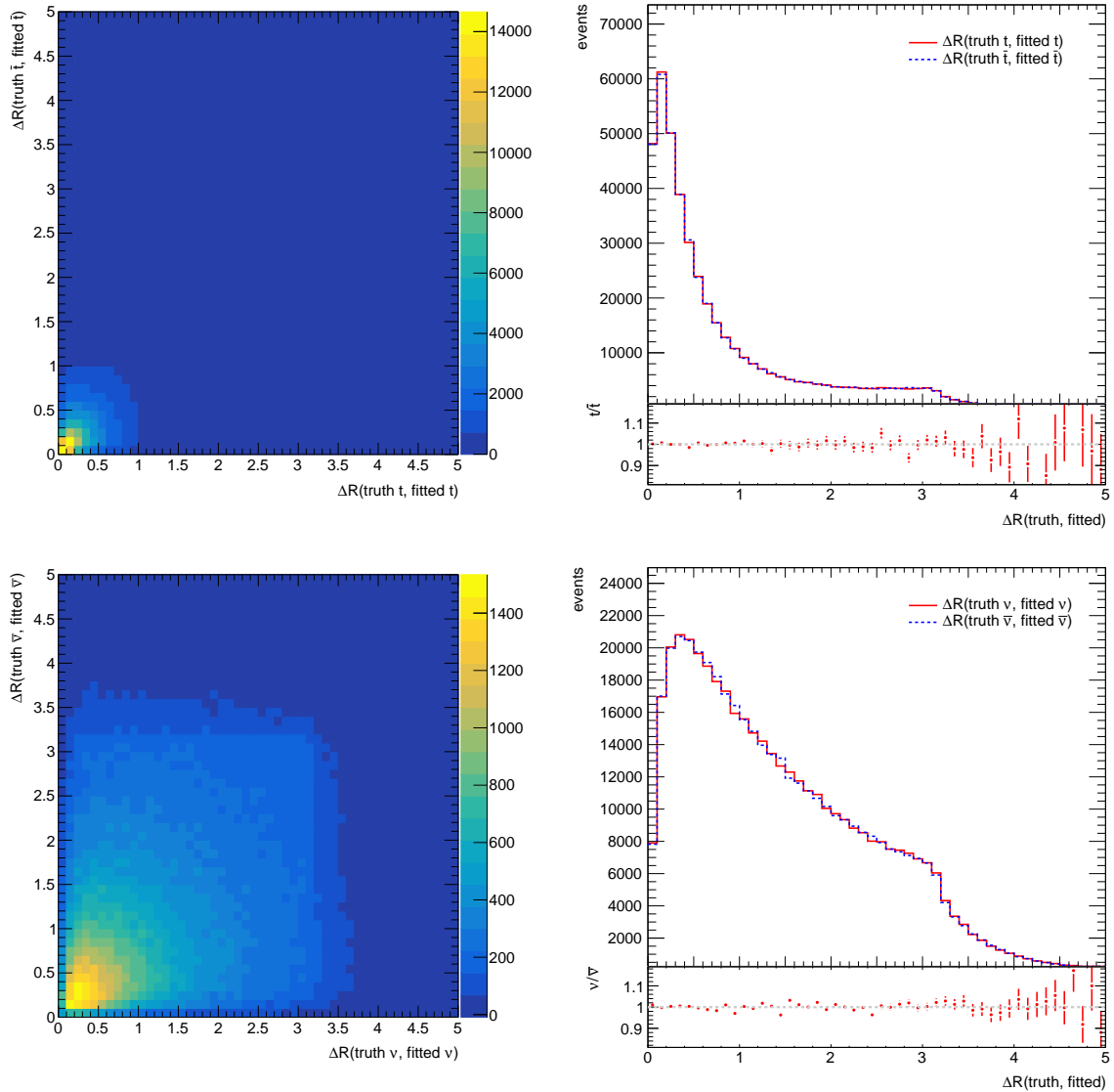
Figure 5.3: Distance ΔR between the truth and fitted top quarks and neutrinos. In the upper histograms, a two-dimensional plot is shown on the left between the top quark on the x- and the antitop quark on the y-axis. Whereas on the right an overlaid histogram is shown for the ΔR distribution of the top quark in red and the antitop quark in dashed blue. In the lower histograms, the same is shown for the neutrino and antineutrino. The kink around $\Delta R = 3$ can be explained by the 2π periodicity of the polar angle φ.

two neutrinos. Calculating the weight has been done by the kinematic reconstruction of the $t\bar{t}$ event, as described in Section 4.1.

For the b-jet and lepton four-momenta, the reco or fitted values can be used. In this analysis, the fitted values show slightly better performances, due to the additional transfer functions which were taken into account. So for the following calculations, these values are used for the reconstruction. Moreover, the top quark mass has to be known and

can either be fixed to $m^t = 172.5\,\text{GeV}$ or varied from the KLFitter framework. Thus, for detector reconstructed values the mass is fixed, whereas for the KLFitter values with transfer functions, the fitted top quark mass is used.

Figure 5.3 shows the distance ΔR between truth and fitted particles, namely top and antitop quark in the upper histograms, as well as neutrino and antineutrino in the lower histograms. The distribution for the top and antitop quark is much narrower compared to the neutrino ΔR distributions, which are much broader. This can be explained by the fact that, in contrast to the neutrino momentum, the top quark four-momentum is the sum of the b-jet, lepton and the neutrino. As shown in Table 5.2, the b-jet and especially the lepton have well-reconstructed four-momentum vectors and they dominate the top quark momentum.

For the top quark, the fraction of events with $\Delta R(\text{truth, fitted}) < 0.4$ is about $47\,\%$ and for the neutrino, the fraction is about $16\,\%$. Almost the same numbers are obtained for the corresponding antiparticles. The fraction for the top quark is compatible with previous studies, whereas for the neutrino, the fraction is about $30\,\%$ less [40].
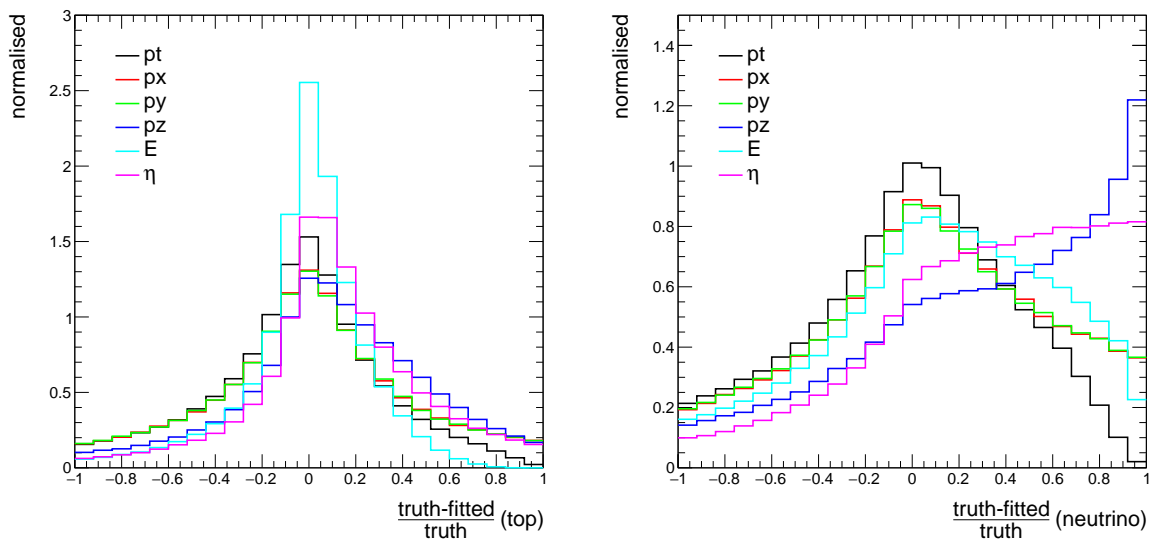

Figure 5.4: Difference for top quark (left) and neutrino (right) between the truth and the fitted values for components p_T, p_x, p_y, p_z, E, η of the corresponding four-momentum vectors.

Figure 5.4 shows the difference per event in the neutrino and top quark four-momenta between truth and fitted, according to $(\text{truth}-\text{fitted})/\text{truth}$ for p_T, p_x, p_y, p_z, E, η. The deviation on the right side of the neutrino histogram, where the fitted value vanishes, can be explained by the assumed pseudorapidity distribution of the neutrino. Similar results

are obtained for the antitop quark and antineutrino.

Keeping the neutrino solution with the highest weight is not implemented within the KLFitter framework. Currently, all the weights for up to four solutions for the neutrino and antineutrino are summed together. For this summed weight, the likelihood is then maximised. A different implementation is developed in this thesis and will be discussed in the following section.

5.4 Comparison of Different Methods

If the neutrino solution with the highest weight is chosen to be the correctly reconstructed one, this must not be the real solution. Even if the highest weight indicates that the missing transverse energy is fulfilled the best by the momentum of the neutrino and antineutrino, it still could be the wrong solution. For this reason, the Neutrino Weighting Algorithm within KLFitter was implemented with the weights summed together in the past.

In the following, a different method will be presented where only the highest weight is taken into account. For this weight, the likelihood is maximised. A comparison between these two methods will be discussed in this section and a conclusion of which one leads to a better performance will be presented.

Weight Statistics In order to classify the weights, certain properties of the weights have been checked as presented in the following. All the numbers are obtained in the case where there are two solutions for the neutrino and the antineutrino, resulting in four calculated weights.

- In approximately $2\,\%$ of the events, all calculated weights are zero (or at least they are too small to match in a `double` variable). So, there is no difference in the methods.

- In $36\,\%$ of the events, three of the four calculated weights vanish. Therefore, again, there is no difference in the two methods. The previous case is a sub-part of this fraction.

- The case, when the weight of one solution is significantly larger than the sum of the remaining three weights, e.g. ten orders of magnitude, happens in approximately $42\,\%$ of the events. Thus, the methods are not equal, but effectively there is no difference in summing the weights and taking only the highest weight.

channels	sum weights			max weight		
	ee	*eμ*	*μμ*	*ee*	*eμ*	*μμ*
both b-jets	65.5 %	66.4 %	67.4 %	67.5 %	68.5 %	69.6 %
b-jet	73.0 %	73.6 %	74.6 %	74.4 %	75.2 %	76.2 %
$\bar{b}$-jet	73.1 %	73.6 %	74.7 %	74.5 %	75.2 %	76.3 %
at least 1 *b*-jet	80.5 %	80.9 %	81.9 %	81.4 %	81.9 %	82.8 %
both leptons	97.6 %	98.4 %	98.7 %	97.6 %	98.4 %	98.7 %

Table 5.3: Reconstruction matching efficiencies for different implementations, either taking the sum of the weights or just the maximum. The values for the sum method are the same as in Table 5.2. The *b*-jet matches the truth *b*-quark if $\Delta R < 0.3$, and the leptons match if both are within $\Delta R < 0.1$ to the truth leptons, as described in Section 5.3.1.

For these analyses, the fitted values are used. The reco values show slightly different results with about 3 to 15 percent more. However, these weight statistics already lead to the assumption that this new method can give at least the same performance, or even better one. Moreover, as mentioned in Section 5.3.2, higher weights could indeed be physically more meaningful.

In the following, the method, in which the weights are summed, is referred as *sum* and taking only the highest weight as *max*.

Efficiencies   The reconstruction efficiencies for both methods are shown in Table 5.3. The efficiencies are calculated in the same way as described in Section 5.3.1, where both leptons are considered matched if $\Delta R < 0.1$ and each *b*-jet if $\Delta R < 0.3$.

With taking the highest weights, the efficiencies increase about two percent compared to the current implementation.

Failing Reconstruction   In the current implementation (sum) the reconstruction of the neutrino fails for almost one fourth of the events when using the fitted values, and for one third of the events for the reco ones. For these events, the term under the square root for the neutrino momentum is negative and thus, it does not have a real solution.

This changes significantly for the newly developed method, as shown in Table 5.4. Especially for the combination of fitted and max, this drops to less than 1 %. When KLFitter found no best permutation, this also decreases slightly (see Section 5.3.2).

Performance   The better performance can be explained by the fact that this combination (fitted and max) is self consistent. In the neutrino reconstruction algorithm, the

	sum weights		max weight	
	reco	fitted	reco	fitted
no best permut. (KLFitter)	0.91%	0.91%	0.89%	0.89%
reconstruction fails (ν)	36.33%	26.16%	22.52%	0.93%

Table 5.4: Fraction of events, when KLFitter finds no best permutation, as described in Section 5.3.2, and fraction of events for a failing reconstruction in the neutrino algorithm, as described in Section 4.1, meaning no real solution due to the quadratic equation.

highest weight is always taken. Hence, if the highest weight is also directly used in KL-Fitter, the method is the same and therefore no contrasting algorithms are utilised.

The new implementation leads to a different output of the neutrino pseudorapidity distribution from KLFitter. To find the best permutation, the Neutrino Weighting Method, which is implemented in the KLFitter framework, calculates a likelihood of all possible variations of pseudorapidities. Thus, a different weight leads to different likelihood functions with different maxima. Hence, the neutrino pseudorapidity output changes. This distribution is used for the neutrino reconstruction as described in Section 4.1 and is shown in Figure 5.5. This is another reason for the decrease in failing events within the neutrino reconstruction (meaning no real solution). Further studies are required to fully understand this significant decrease.
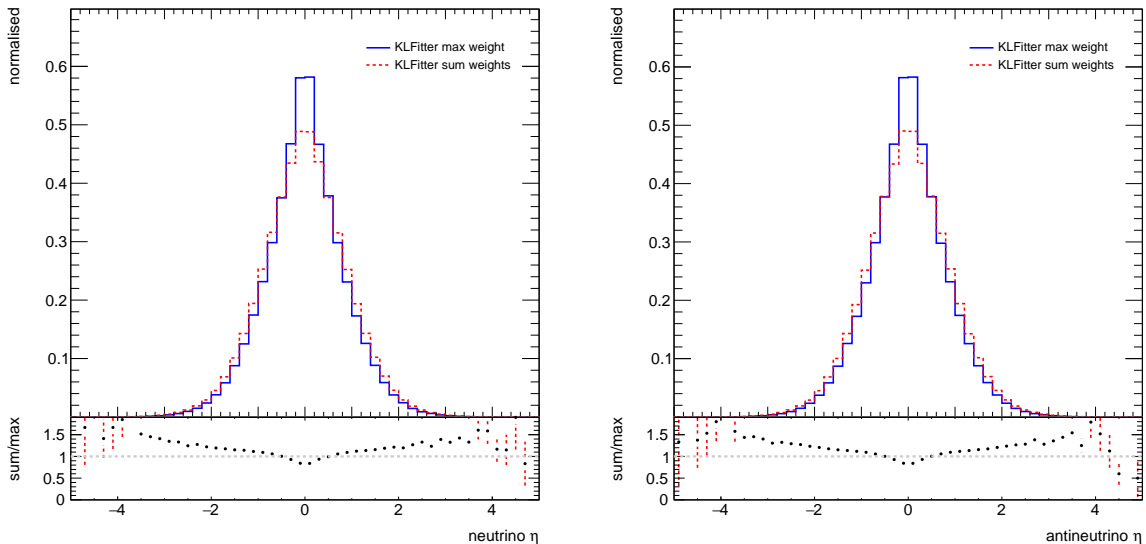

Figure 5.5: Different KLFitter output for the neutrino (left) and antineutrino (right) pseudorapidity distributions for the two different implemented methods, namely summing the weights (in dashed red) and taking only the maximum of the weights (in blue).

5.5 Running on Background Sample

As discussed in the previous section, implementing the new method results in an increase in the performance and efficiency. To check if that only happens on the signal sample and leads to worse statistics in the Wt background, further studies were made. The logarithm of the likelihood is plotted for the background using both methods, shown in Figure 5.6. The difference is small, within a justifiable range, and indicates only larger deviations for the low statistic region.

The reconstruction fails, meaning no real solution of the neutrino momentum, for about 20.2% of the events when the sum method is used (in the signal 26.2%) and in the max method for about 0.8% (in the signal 0.9%). The fitted values are used.
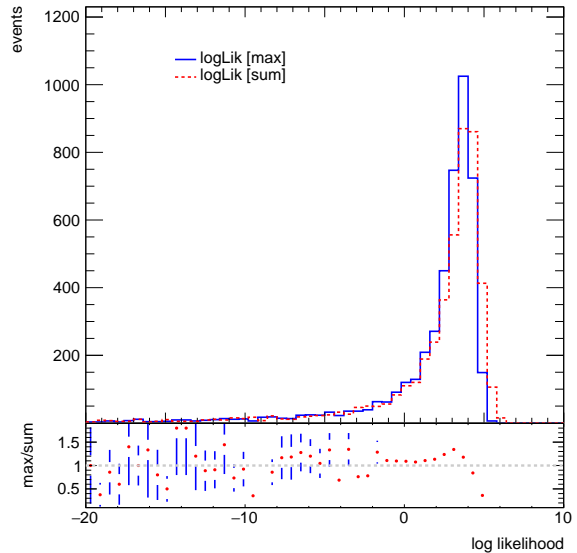

Figure 5.6: Comparison between the sum (dashed red) and the max (blue) methods for the logarithm of the likelihood in the Wt background.

5.6 Tuning Parameter

To verify the increase of the reconstruction efficiency due to the tuning parameter α, the cases where $\alpha = -2$ and $\alpha = 0$ are compared, effectively turning off the additional term in the latter one. This tuning parameter is in the likelihood (see Equation (4.17)) as an additional mass term and increases the likelihood. In Section 4.3 it is mentioned, that the best separation for the correct assignment to the top and antitop quark is provided by $\alpha = -2$ [40]. Table 5.5 shows the comparison of these two options for the tuning parameter for both methods – summing the weights and taking only the highest weight. And indeed, the efficiencies decrease slightly for $\alpha = 0$. However, a physical justification for this tuning parameter is still necessary and further studies regarding this topic are required. The efficiencies are almost the same, when the tuning parameter is dropped and instead, the method with the highest weight is taken. So if one wants to proceed without that additional parameter, but keeping almost the same reconstruction efficiencies, the new method developed within this thesis (max) is the preferred option.

	sum weights		max weight	
	$\alpha = -2$	$\alpha = 0$	$\alpha = -2$	$\alpha = 0$
both b-jets	66.5%	66.0%	68.6%	67.7%
b-jet	73.7%	71.9%	75.3%	73.9%
$\bar{b}$-jet	73.8%	72.0%	75.3%	73.9%
at least 1 b-jet	81.1%	78.9%	82.0%	80.1%
both leptons	98.3%	98.3%	98.3%	98.3%

Table 5.5: Efficiencies for different tuning parameters α and methods (sum/max).

5.7 Using new Transfer Functions

A last additional study in this thesis, regarding the research on reconstruction of $t\bar{t}$ dilepton events, is done for the usage of new Transfer Functions (TF) at $\sqrt{s} = 13\,\text{TeV}$. They describe higher order effects and detector resolution, as discussed in Section 4.3. This should lead to a more precise modelling of the missing transverse energy as it would appear in the detector. Furthermore, the reconstructed b-jets and leptons should also show a better modelling.

	sum weights		max weight	
	old TF	new TF	old TF	new TF
both b-jets	66.5%	65.8%	68.6%	67.6%
b-jet	73.7%	73.4%	75.3%	74.7%
$\bar{b}$-jet	73.8%	73.4%	75.3%	74.8%
at least 1 b-jet	81.1%	80.9%	82.0%	81.9%
both leptons	98.3%	98.1%	98.3%	98.1%

Table 5.6: Efficiencies for different transfer functions (TF) and methods (sum/max).

However, with the new TF, the efficiencies decrease slightly, as it is shown in Table 5.6. But these differences are less than one percent and can be effected by other reasons. For example, the TF used in this thesis were developed with data conditions from 2015. The new TF with the full Run II conditions are still under development and thereby could not be used for this thesis.

Moreover, none of the two methods perform any better with these new TF. Thus, there is no disadvantage in using the new method, where just the maximum of the weight is taken.

32

6 Conclusion and Outlook

In this thesis, the kinematic reconstruction of $t\bar{t}$ dileptonic events is studied. The Neutrino Weighting Method is used, which is implemented in the KLFitter framework. In the dileptonic channel, due to the presence of two undetected neutrinos, the reconstruction is challenging. The kinematic system is underconstrained and therefore, assumptions are necessary.

First, the neutrino pseudorapidity distribution is updated for the centre-of-mass energy of $\sqrt{s} = 13\,\text{TeV}$. The MC truth η distribution is approximated by a Gaussian function and the resulting σ is implemented in the KLFitter framework. For the higher available centre-of-mass energy of the LHC, that σ increases and therefore, the neutrino pseudorapidity distribution gets broader. The obtained Gaussian fit is within statistical errors. With the updated pseudorapidity distributions, the kinematic reconstruction is performed, as described in Chapter 4. However, due to the quadratic nature of the final neutrino momentum equations, there remains an ambiguity of up to four solutions. In this thesis, a method when only the neutrino with the highest weight in Equation (5.1) is kept as the correctly reconstructed one, is presented.

The new method shows a better performance and reconstruction matching efficiency for the b-jets and leptons. Even the number of events in cases where the reconstruction fails, meaning no real solution for the neutrino momentum due to the quadratic equation, decreases significantly – from $26\,\%$ to less than $1\,\%$. The Neutrino Weighting Method provides only a unique solution of the neutrino, if one out of the four possibilities is chosen. In this thesis, it is shown for the highest weight. Certainly, further studies can be made in order to see if the highest weight is indeed the best choice and if maybe other selections of the correctly reconstructed neutrino can lead to even better results.

The studies of the background have shown that the new implementation does not decrease the matching efficiency. Almost the same number of events, when the reconstruction fails, was obtained in the Wt background, and the likelihood function changes negligibly. Thus, the signal as well as the background leads to better efficiencies with the new method when only the maximum of the weights is taken into account.

The verification of the tuning parameter α has shown that it increases slightly the reconstruction efficiency. However, for a deeper verification of that tuning parameter, further studies are required.

The usage of new transfer functions at $\sqrt{s} = 13\,\mathrm{TeV}$ does not, in contrast to the expectations, lead to better efficiencies. Although, these deviations lie under a percentage range and can be affected by various other reasons, e.g. not the latest transfer functions. Therefore, the results that are obtained in this thesis, will not be affected significantly by the fully developed transfer function and will be still valid.

With the new approach of taking only the highest weight directly in the KLFitter framework, it is possible to save the reconstructed neutrino and provide it for the user in the output. For that, a new particle *neutrino* could be added in the KLFitter code, where the four-momentum of the neutrino is saved. Hence, the full momenta of all particles in the final state can be available in the output.

The fully reconstructed $t\bar{t}$ dilepton system can be used for many top quark measurements, such as the top quark mass or other properties of the $t\bar{t}$ system in the dileptonic channel.

Bibliography

[1] S. L. Glashow, *Partial Symmetries of Weak Interactions*, Nucl. Phys. **22**, 579 (1961)

[2] M. Gell-Mann, *A Schematic Model of Baryons and Mesons*, Phys. Lett. **8** (1964)

[3] S. Weinberg, *A Model of Leptons*, Phys. Rev. Lett. **19**, 1264 (1967)

[4] A. Salam, *Weak and Electromagnetic Interactions*, Proceedings of the 8th Nobel symposium, Ed. N. Svartholm, Almqvist & Wiskell, 1968, Conf. Proc. **C680519**, 367 (1968)

[5] S. L. Glashow, J. Iliopoulos, L. Maiani, *Weak Interactions with Lepton-Hadron Symmetry*, Phys. Rev. **D2**, 1285 (1970)

[6] G. 't Hooft, M. J. G. Veltman, *Regularization and Renormalization of Gauge Fields*, Nucl. Phys. **B44**, 189 (1972)

[7] M. Kobayashi, T. Maskawa, *CP Violation in the Renormalizable Theory of Weak Interaction*, Prog. Theor. Phys. **49**, 652 (1973)

[8] ATLAS Collaboration, *Observation of a new particle in the search for the Standard Model Higgs boson with the ATLAS detector at the LHC*, Phys. Lett. **B716**, 1 (2012)

[9] CMS Collaboration, *Observation of a new boson at a mass of 125 GeV with the CMS experiment at the LHC*, Phys. Lett. **B716**, 30 (2012)

[10] M. Thomson, *Modern Particle Physics*, Cambridge University Press (2013)

[11] D. Griffiths, *Introduction to Elementary Particles*, Wiley-VCH (2008)

[12] F. Englert, R. Brout, *Broken symmetry and the mass of gauge vector mesons*, Phys. Rev. Lett. **13**, 321 (1964)

[13] P. W. Higgs, *Broken symmetries, massless particles and gauge fields*, Phys. Lett. **12**, 132 (1964)

[14] P. W. Higgs, *Broken symmetries and the masses of gauge bosons*, Phys. Rev. Lett. **13**, 508 (1964)

[15] G. Guralnik, C. Hagen, T. Kibble, *Global conservation laws and massless particles*, Phys. Rev. Lett. **13**, 585 (1964)

[16] P. W. Higgs, *Spontaneous symmetry breakdown without massless bosons*, Phys. Rev. **145**, 1156 (1966)

[17] T. Kibble, *Symmetry breaking in non-Abelian gauge theories*, Phys. Rev. **155**, 1554 (1967)

[18] Y. Fukuda, et al. (Super-Kamiokande), *Evidence for oscillation of atmospheric neutrinos*, Phys. Rev. Lett. **81**, 1562 (1998)

[19] M. Kobayashi, T. Maskawa, *CP Violation in the Renormalizable Theory of Weak Interaction*, Prog. Theor. Phys. **49**, 652 (1973)

[20] F. Abe, et al. (CDF Collaboration), *Observation of top quark production in $\bar{p}p$ collisions*, Phys. Rev. Lett. **74**, 2626 (1995)

[21] S. Abachi, et al. (DØ Collaboration), *Search for high mass top quark production in $p\bar{p}$ collisions at $\sqrt{s} = 1.8$ TeV*, Phys. Rev. Lett. **74**, 2422 (1995)

[22] C. Patrignani, et al. (Particle Data Group), *Review of Particle Physics*, Chin. Phys. **C40(10)**, 100001 (2016)

[23] A. Quadt, *Top quark physics at hadron colliders*, Eur. Phys. J. **C48**, 835 (2006)

[24] T. Aaltonen, et al. (CDF Collaboration), *Observation of Electroweak Single Top-Quark Production*, Phys. Rev. Lett. **103**, 092002 (2009)

[25] V. M. Abazov, et al. (DØ Collaboration), *Observation of Single Top Quark Production*, Phys. Rev. Lett. **103**, 092001 (2009)

[26] L. Evans, P. Bryant, *LHC Machine*, JINST **3**, S08001 (2008)

[27] ATLAS Collaboration, *The ATLAS Experiment at the CERN LHC*, JINST **3**, S08003 (2008)

[28] CMS Collaboration, *The CMS Experiment at the CERN LHC*, JINST **3**, S08004 (2008)

[29] LHCb Collaboration, *The LHCb Detector at the LHC*, JINST **3**, S08005 (2008)

[30] ALICE Collaboration, *The ALICE experiment at the CERN LHC*, JINST **3**, S08002 (2008)

[31] LHCf Collaboration, *The LHCf detector at the CERN Large Hadron Collider*, JINST **3**, S08006 (2008)

[32] TOTEM Collaboration, *The TOTEM experiment at the CERN Large Hadron Collider*, JINST **3**, S08007 (2008)

[33] J. L. Pinfold, *The MoEDAL experiment at the LHC - A new light on the high energy frontier*, Mod. Phys. Lett. **A29**, 1430003 (2014)

[34] S. Frixione, P. Nason, C. Oleari, *Matching NLO QCD computations with Parton Shower simulations: the POWHEG method*, JHEP **11**, 070 (2007)

[35] T. Sjöstrand, S. Mrenna, P. Z. Skands, *A Brief Introduction to PYTHIA 8.1*, Comput. Phys. Commun. **178**, 852 (2008)

[36] T. Sjöstrand, S. Mrenna, P. Z. Skands, *PYTHIA 6.4 Physics and Manual*, JHEP **05**, 026 (2006)

[37] B. Abbott, et al. (DØ Collaboration), *Measurement of the top quark mass using dilepton events*, Phys. Rev. Lett. **80**, 2063 (1998)

[38] B. Abbott, et al. (DØ Collaboration), *Measurement of the Top Quark Mass in the Dilepton Channel*, Phys. Rev. **D60**, 052001 (1999)

[39] J. Erdmann, et al., *A likelihood-based reconstruction algorithm for top-quark pairs and the KLFitter framework*, Nucl. Instrum. Meth. **A748**, 18 (2014)

[40] T. Vazquez Schröder, *Measurement of the associated production of a vector boson (W, Z) and top quark pair in the opposite sign dilepton channel with pp collisions at $\sqrt{s} = 8$ TeV with the ATLAS detector*, Ph.D. thesis, Göttingen U., CERN-THESIS-2014-225, II.Physik-UniGö-Diss-2014/06, II. Phys. Inst. (2014)

[41] P. Calafiura, et al., *The Athena control framework in production, new developments and lessons learned*, Interlaken, CHEP pages 456–458 (2005)

[42] ATLAS Collaboration, *Performance of b-Jet Identification in the ATLAS Experiment*, JINST **11(04)**, P04008 (2016)

Danksagung

Zuerst möchte ich einen großen Dank an meinen Erstgutachter und Betreuer der Bachelorarbeit aussprechen – Prof. Dr. Arnulf Quadt, der mir die Möglichkeit gegeben hat, im II. Physikalischen Institut an der Georg-August Universität Göttingen die Bachelorarbeit schreiben zu können. Dadurch konnte ich einen Einblick in die Welt der Teilchenphysik sowie die des LHC und ATLAS Experiments gewinnen. Vielen Dank dafür. Ebenso danke ich Prof. Dr. Ariane Frey für die Zweitkorrektur dieser Arbeit.

Des Weiteren möchte ich Dr. Royer Edson Ticse Torres und Ishan Pokharel danken, die mich unterstützt haben und jederzeit bei Fragen zur Verfügung standen. Gab es mal Schwierigkeiten oder Phasen des Stillstands, so haben sie mir immer wieder neue Anregungen und Hilfestellungen gegeben.

Vielen Dank auch an alle Mitglieder des II. Physikalischen Instituts, insbesondere jene, die an der Korrekturlesung dieser Bachelorarbeit beteiligt waren und mir viele hilfreiche Kommentare gaben.

Schlussendlich möchte ich noch meiner Familie und besonders meinen Eltern danken, die mich über die gesamte Zeit des Bachelorstudiums hinweg unterstützt und dieses überhaupt so erst ermöglicht haben.

Erklärung   nach §13(9) der Prüfungsordnung für den Bachelor-Studiengang Physik und den Master-Studiengang Physik an der Universität Göttingen:

Hiermit erkläre ich, dass ich diese Abschlussarbeit selbständig verfasst habe, keine anderen als die angegebenen Quellen und Hilfsmittel benutzt habe und alle Stellen, die wörtlich oder sinngemäß aus veröffentlichten Schriften entnommen wurden, als solche kenntlich gemacht habe.

Darüberhinaus erkläre ich, dass diese Abschlussarbeit nicht, auch nicht auszugsweise, im Rahmen einer nichtbestandenen Prüfung an dieser oder einer anderen Hochschule eingereicht wurde.

Göttingen, den 16. Juli 2018

(Maximilian Stephan Kurjahn)